A Two-Input Sliding-Mode Controller for a Planar Arm Actuated by Four Pneumatic Muscle Groups

John H. Lilly and Peter M. Quesada

***Abstract*—Multiple-input sliding-mode techniques are applied to a planar arm actuated by four groups of pneumatic muscle (PM) actuators in opposing pair configuration. The control objective is end-effector tracking of a desired path in Cartesian space. The inputs to the system are commanded input pressure differentials for the two opposing PM groups. An existing model for the muscle is incorporated into the arm equations of motion to arrive at a two-input, two-output nonlinear model of the planar arm that is affine in the input and, therefore, suitable for sliding-mode techniques. Relationships between static input pressures are derived for suitable arm behavior in the absence of a control signal. Simulation studies are reported.**

***Index Terms*—Pneumatic muscle actuators, robotics, sliding-mode control.**

I. Introduction

PNEUMATIC actuators have been used for many years to provide motive power to many mechanical systems, including robots. One relatively new type of pneumatic actuator, the McKibben artificial muscle, or pneumatic muscle (PM), possesses all the advantages of traditional pneumatic actuators (i.e., light weight, low cost) without the main drawback (i.e., low power-to-weight ratio). A PM consists of a cylindrical flexible rubber or plastic airtight tube that fits snugly inside a braided plastic sheath with helical winding (see Fig. 1). When the tube is inflated, it widens and due to the braided sheath, shortens. The axial force exerted when the PM shortens is quite large in proportion to the PM's weight. Pneumatic muscles have the highest power/weight and power/volume ratios of any actuator [1], [2].

PMs can be made similar to human skeletal muscles in size, weight, and power output. Their high power/weight and power/volume ratios, in conjunction with their contractile nature (i.e., their inherent extensibility when activated), could make these actuators extremely useful in a variety of rehabilitation engineering applications for persons with neuromuscular or musculoskeletal pathologies that affect extremity function. Disorders that limit or hinder extremity function can include stroke, traumatic brain injury, amputation, and spinal cord injury. These conditions are associated with a number of physical challenges, including weakness, paralysis, limb loss, and joint contracture associated with spasticity and/or hypertonia. Individuals with such challenges could potentially benefit from powered devices that provide joint loading to generate or assist extremity motion, or maintain extension of muscles with contractures.

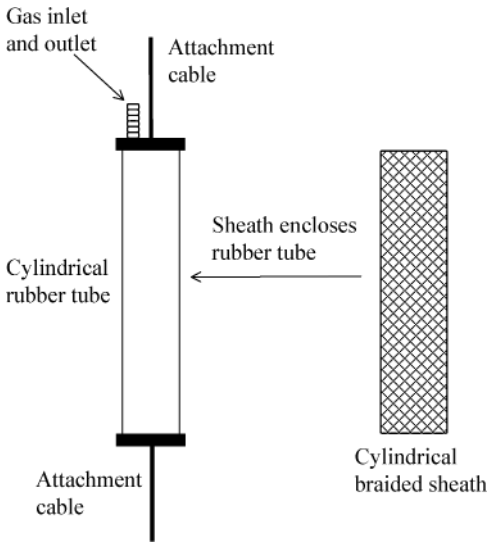

Fig. 1. Construction of PM actuator.

Many potential applications involve some type of exoskeletal or link segment configuration that attaches to existing anatomical body segments [3]–[7]. Devices of these types have often been relegated to use within a specific location (i.e., laboratory setting), or have limited actuation to small segments at the hand/wrist. Lower power-to-volume ratios of traditionally used power sources could hinder the use of powered exoskeletal orthoses, for larger extremity segments, in more general settings. Utilization of PMs to power exoskeletal devices, which interface with persons who have functional deficits, could potentially reduce size and weight sufficiently to facilitate more widespread use of such devices.

It should also be noted that traditional actuators, such as electric motors, are typically rigid in nature. Such actuators can create uncomfortable or painful conditions when interfacing with humans. For example, if an exoskeletal brace, actuated by a stepper motor pulley arrangement, is activated to extend a contracted joint to some desired angle, and a flexor spasticity episode occurs, the stepper motor will rigidly hold its position and not permit joint flexion. Such a response could result in pain and discomfort among patients with joint contractures associated with spasticity. Conversely, activated PMs maintain inherent extensibility, which could permit some joint flexion during muscular loading due to episodes of spasticity. While the elastic properties of PMs can complicate the control aspects of these actuators, they can potentially contribute to more comfortable devices when interfacing with human limb segments.

Manuscript received December 28, 2003; revised April 27, 2004. This work was supported by the Air Force Office of Scientific Research under Grant F49620-00-1-0300 and by the Kentucky Science and Engineering Foundation under Grant 148-502-02-37.

J. H. Lilly is with the Department of Electrical and Computer Engineering, University of Louisville, Louisville, KY 40292 USA.

P. M. Quesada is with the Department of Mechanical Engineering, University of Louisville, Louisville, KY 40292 USA.

Digital Object Identifier 10.1109/TNSRE.2004.831490

Research into the physical and modeling properties of PMs has been undertaken at the INSA (Toulouse, France) [8], the BioRobotics Lab at the University of Washington, Seattle, [9], and the Human Sensory Feedback (HSF) Laboratory at Wright Patterson Air Force Base [10], among others. Of particular interest in our research are the modeling results of [10], which cast the PM as a parallel connection of a nonlinear spring, dashpot, and contractile element. All three components in the model have coefficients that depend nonlinearly on the commanded PM pressure. The resulting mathematical model is a second-order nonlinear time-varying differential equation.

This paper addresses the control of a two-joint planar robotic arm actuated by four groups of PMs. Due to their highly nonlinear and time-varying nature, PM control presents a challenging nonlinear control problem that has been approached via many methodologies. In [11], a direct continuous-time adaptive control technique is applied to control joint angle in a single-joint arm. The simulation considers PMs individually in both bicep and tricep positions. In [12], an indirect discrete adaptive controller is used to control an antagonistic PM pair actuating an actual robotic arm in the lab. In [13], an antagonistic PM pair actuates a leg-like swinging pendulum in the lab. The PMs are actuated in periodic fashion to mimic walking movements, and the action is controlled by a proportional digital pole-placement controller. In [14], PMs are used in the actuation of a hand-like manipulator in the lab. A linear discrete model of the process is identified offline via least squares, and a discrete pole-placement controller with integral action is designed.

In [15], a five-link robot in the lab is controlled by a neural network using backpropagation to learn the correct control over a period of time. In [16], a gain scheduling controller is designed for a single PM hanging vertically in the lab actuating a mass. Both force and position control are considered. In [17], a fuzzy model reference learning controller is designed for a single PM hanging vertically actuating a mass in the lab. Tracking results are obtained, and these are shown to agree well with simulated results. In [18], a fuzzy P+ID controller is designed for the system of [17] using an evolutionary algorithm. Also included is a new method of identifying fuzzy systems from experimental data using evolutionalry techniques. The experimental results are shown to be superior to those in [17], i.e., tracking error is less while using less control effort. In [19], a backstepping controller using fuzzy techniques to determine valve status is designed for a simulation of a PM hanging vertically in the lab. In [20], sliding-mode control is applied to a three degree-of-freedom (DOF) PM-actuated anthropomorphic manipulator in the lab. Sliding mode control is also used in [21] and [22]. In [23], H_∞ methods are used for PM control.

In this paper, we consider a multiple-input sliding-mode approach [24]–[27] to control a two-joint planar arm with four PMs in antagonist pairs. Sliding control has the advantage that it can provide accurate tracking with bounded error in the presence of model uncertainties. Sliding mode control is ideal for PM manipulation because the PM model is usually poorly known, nonlinear, and time-varying, necessitating some type of robust control strategy. This also accounts for the success of adaptive, variable-structure, and soft computing approaches.

The contributions of this paper include modeling of the arm with four groups of PM actuators, formulating the model so that it is suitable for sliding-mode control, determination of static pressures for stable arm behavior in the absence of a control signal, and simulation results of varying the PM coefficients and the mass actuated by the arm.

This paper is arranged as follows. Section II contains a discussion of the PM mathematical model used in this paper. Section III derives the model of a planar arm actuated by four groups of PMs in antagonistic pair configuration. Section IV addresses the problem of guaranteeing stable arm behavior in the absence of a control signal. Section V presents the derivation of a two-input sliding-mode controller for the arm. Section VI presents simulations of the closed-loop tracking performance of the controller. Section VII contains discussion and conclusions.

II. Planar Arm Dynamic Model

In this paper, we consider PMs of the type modeled in [10] and shown in Fig. 1. This particular PM has an inner bladder made from a section of 22.2-mm-diameter bicycle tubing enclosed in a helically wound nylon sheath used for supporting electrical cables. The unstretched, uncompressed diameter of the sheath is 31.75 mm. The PM is inflated by supplying voltage to a solenoid that controls the flow of pressurized gas into the rubber bladder. It is deflated by exciting another solenoid venting the contents of the bladder to the atmosphere. When inflated, the PM shortens via the action of the braided nylon sheath, exerting a contractile force that is quite large in proportion to the PM's weight.

The dynamic behavior of this particular PM hanging vertically actuating a mass has been modeled as a combination of a nonlinear friction, a nonlinear spring, and a nonlinear contractile element [10], although other approaches to modeling also exist [8], [9]. See [10] for a complete description of this PM. The coefficients corresponding to these three elements depend on the input pressure P of the PM. The coefficient of friction B, in addition, also depends on whether the PM is being inflated or deflated. The latter property is because deflation is easier since air pressure only has to work against a constant atmospheric pressure. However, during inflation, the air pressure must work against a source that is constantly changing in pressure, hence it is much more difficult and nonlinear.

As in [10], let $x(t)$ be the amount of PM contraction, with $x = 0$ corresponding to the PM being fully deflated (defined as 206.85 kPa, or 30 psi) and lengthened and x increasing as the PM contracts. Then, the equation describing the dynamics of this PM hanging vertically actuating a mass is

$$M\ddot{x} + B(P)\dot{x} + K(P)x = F(P) - Mg \tag{2.1}$$

where the coefficients $K(P)$, $B(P)$, and $F(P)$ are given in [10] as

$$\begin{aligned} K(P) &= K_0 + K_1 P \\ &= 5.71 + 0.0307P \end{aligned} \tag{2.2}$$

$$\begin{aligned} B(P) &= B_{0i} + B_{1i} P \\ &= 1.01 + 0.00691P \quad \text{(inflation)} \end{aligned} \tag{2.3a}$$

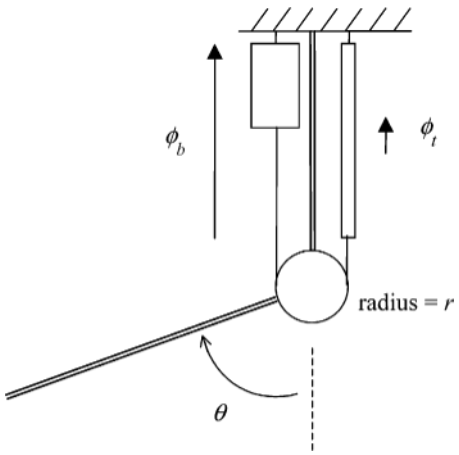

Fig. 2. Two PMs tied together around a pulley.

$$B(P) = B_{0d} + B_{1d}P = 0.6 - 0.000\,803P \quad \text{(deflation)} \tag{2.3b}$$

$$F(P) = F_0 + F_1P = 179.2 + 1.39P. \tag{2.4}$$

It is stated in [10] that these coefficients are appicable for pressures in the range $206.844 \leq P \leq 620.532$ kPa $(30 \leq P \leq 90$ psi$)$.

We note that the nonlinear spring and damping coefficients, as well as the contractile element depend on the PM input pressure P, which is the pressure in the inlet hose to the PM. It is the control variable to the PM that can be exactly commanded by the controller via an internal closed-loop system that assures that P is always exactly proportional to the current delivered to the inlet valve. Therefore, the control signal enters this system not only in the normal way (through F), but also through the spring and damping coefficients, which is rather unusual for control.

From (2.1), the total force exerted by the PM on the mass is

$$\phi = F(P) - B(P)\dot{x} - K(P)x. \tag{2.5}$$

If several PMs are present in a system, each one generally has its own F, K, and B coefficients, its own input pressure P, and its own inflation or deflation status.

Assume we have a pair of such PMs tied together around a pulley of radius r as in Fig. 2, with the connecting line rigidly attached to the pulley to prevent slipping. Then, the torque imparted to the pulley by the PM pair is

$$\tau_{\text{total}} = \tau_b - \tau_t = (\phi_b - \phi_t)r \tag{2.6}$$

where τ_b and τ_t are the torques due to each individual PM and are given by

$$\tau_b = (F_b - K_bx_b - B_b\dot{x}_b)r \tag{2.7a}$$

$$\tau_t = (F_t - K_tx_t - B_t\dot{x}_t)r. \tag{2.7b}$$

In (2.7), x_b is the length of PM b and x_t is the length of PM t. The lengths of the arrows in Fig. 2 are indicative of the forces exerted by the two PMs. Thus, $\phi_b > \phi_t$ and the torque exerted on the joint is clockwise. The total torque delivered to the pulley is given by

$$\tau_{\text{total}} = (F_b - K_bx_b - B_b\dot{x}_b - F_t + K_tx_t + B_t\dot{x}_t)r \tag{2.8}$$

where F_b, K_b, and B_b depend on the input pressure of PM b and F_t, K_t, and B_t depend on the input pressure of PM t according to (2.2)–(2.4).

The lengths x_b, x_t can be expressed in terms of the pulley angle θ since the pulley radius is known. We will find it advantageous to do so in order to formulate a two-input sliding-mode controller for the planar arm actuated by opposing-pair PMs.

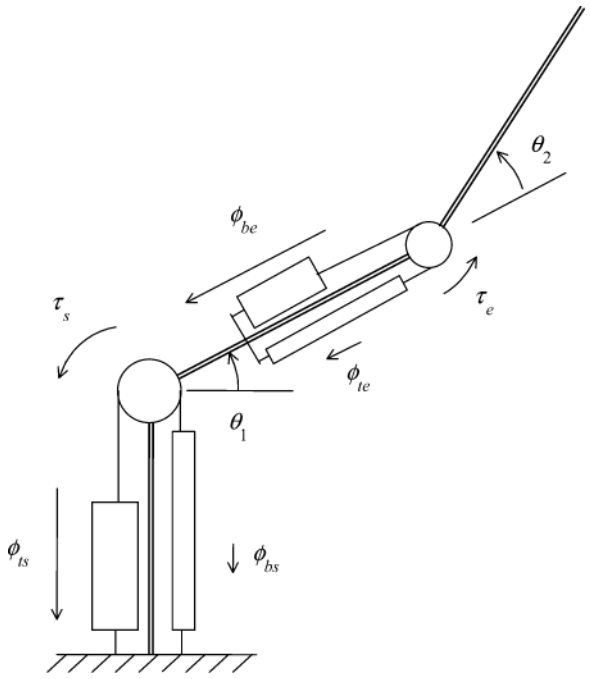

Fig. 3. Arm with PMs.

III. Dynamics of Planar Arm Actuated by PMs

The arrangement of PMs on the manipulator is shown in Fig. 3. The base (or torso) is fixed. At the top of the torso is the shoulder revolute joint, which is rigidly attached to a concentric pulley. The upper arm is attached to the shoulder joint, which is rotatable through an angle $-(\pi/2) < \theta_1 < (\pi/2)$. At the end of the upper arm is the elbow revolute joint, which is rigidly attached to a concentric pulley. The forearm is attached to the elbow joint, which is free to rotate through an angle $0 < \theta_2 < \pi$.

Assume there are n_s pairs of matched PMs (i.e., all PMs have identical coefficients and lengths) tied together around the shoulder pulley (radius r_s) with all tricep PMs recieving the same input pressure P_{ts} and all bicep PMs recieving the same input pressure P_{bs}. Similarly, assume there are n_e pairs of matched PMs tied together around the elbow pulley (radius r_e) with all tricep PMs recieving the same input pressure P_{te} and all bicep PMs recieving the same input pressure P_{be}. We do not assume the elbow PMs are matched to the shoulder PMs, however. The assumption of matched PMs is rather idealistic. However, if care is taken to keep construtions of individual

PMs the same and of the same materials and dimensions, the assumption of matched PMs may not be too erroneous. Consideration of nonmatched PMs is beyond the scope of this paper.

Under these conditions, the shoulder and elbow torques τ_s and τ_e can be expressed using (2.8)

$$\begin{aligned}\tau_s =& n_s(F_s - K_s x_{ts} - B_{ts}\dot{x}_{ts} - F_s \\ &+ K_s x_{bs} + B_{bs}\dot{x}_{bs})r_s \qquad (3.1a)\\ \tau_e =& n_e(F_e - K_e x_{be} - B_{be}\dot{x}_{be} - F_e \\ &+ K_e x_{te} + B_{te}\dot{x}_{te})r_e \qquad (3.1b)\end{aligned}$$

where F_s, K_s, B_{ts}, and B_{bs} (F_e, K_e, B_{te}, and B_{be}) are the coefficients for the shoulder (elbow) PMs, t subscripts denote tricep PM quantities, b subscripts denote bicep PM quantities, s subscripts denote shoulder PM quantities (i.e., PMs located on the torso actuating the shoulder), and e subscripts denote elbow PM quantities (i.e., PMs located on the upper arm actuating the elbow).

A shoulder angle of $\theta_1 = -\pi/2$ corresponds to the shoulder tricep PMs being fully lengthened and the shoulder bicep PMs being fully shortened, and $\theta_1 = +\pi/2$ corresponds to the shoulder tricep PMs being fully shortened and the shoulder bicep PMs being fully lengthened. Therefore, the PM lengths x_{ts} and x_{bs} can be expressed in terms of θ_1 as

$$x_{ts} = r_s\left(\theta_1 + \frac{\pi}{2}\right) \qquad (3.2a)$$

$$x_{bs} = r_s\left(\frac{\pi}{2} - \theta_1\right). \qquad (3.2b)$$

Similarly, with $\theta_2 = 0$ corresponding to full shortening of the elbow tricep PMs and full lengthening of the elbow bicep PMs, and $\theta_2 = \pi$ corresponding to full lengthening of the elbow tricep PMs and full shortening of the elbow bicep PMs, the PM lengths x_{te} and x_{be} can be expressed in terms of θ_2 as

$$x_{te} = r_e(\pi - \theta_2) \qquad (3.3a)$$

$$x_{be} = r_e\theta_2. \qquad (3.3b)$$

Let the input pressure of the shoulder bicep and tricep PMs be

$$P_{bs} = P_{0bs} + \Delta p_s \qquad (3.4a)$$

$$P_{ts} = P_{0ts} - \Delta p_s \qquad (3.4b)$$

where P_{0bs} and P_{0ts} are arbitrary positive nominal constant pressures and Δp_s is an arbitrary function of time that is commanded by the controller. With these definitions, the set of n_s shoulder antagonist pair*s* becomes a single-input system with input Δp_s. When the bicep input pressure increases, the tricep input pressure decreases and *vice versa*, varying the torque on the shoulder joint. The nominal constant pressures P_{0bs} and P_{0ts} are arbitrary and can be chosen so that 1) the shoulder joint is well-behaved in the absence of a control signal Δp_s and 2) desired joint stiffness is produced (see Section IV). Similarly, let the input pressures of the elbow PMs be defined as

$$P_{be} = P_{0be} + \Delta p_e \qquad (3.5a)$$

$$P_{te} = P_{0te} - \Delta p_e \qquad (3.5b)$$

where P_{0be} and P_{0te} are arbitrary positive nominal constant pressures. With these definitions, the set of n_e elbow antagonist pairs becomes a single-input system with input Δp_e. Thus, with the input pressures defined as in (3.4) and (3.5), the 2-DOF planar arm of Fig. 3 is a two-input system with input Δp_s determining the shoulder torque τ_s and input Δp_e determining the elbow torque τ_e.

With definitions (3.1)–(3.5), we can write the shoulder and elbow torques as

$$\tau_s = \tau_{0s} + \tau_{1s}\Delta p_s \qquad (3.6a)$$

$$\tau_e = \tau_{0e} + \tau_{1e}\Delta p_e \qquad (3.6b)$$

where

$$\begin{aligned}\tau_{0s} =& n_s\,[F_{0s} + F_{1s}P_{0ts} - (K_{0s} + K_{1s}P_{0ts}) \\ &\times x_{ts} - (B_{0ts} + B_{1ts}P_{0ts})\dot{x}_{ts} \\ &- F_{0s} - F_{1s}P_{0bs} + (K_{0s} + K_{1s}P_{0bs}) \\ &\times x_{bs} + (B_{0bs} + B_{1bs}P_{0bs})\dot{x}_{bs}]\,r_s \qquad (3.7a)\\ \tau_{1s} =& n_s[-F_{1s} + K_{1s}x_{ts} - B_{1ts}\dot{x}_{ts} \\ &- F_{1s} + K_{1s}x_{bs} + B_{1bs}\dot{x}_{bs}]r_s \qquad (3.7b)\\ \tau_{0e} =& n_e\,[F_{0e} + F_{1e}P_{0be} - (K_{0e} + K_{1e}P_{0be}) \\ &\times x_{be} - (B_{0be} + B_{1be}P_{0be})\dot{x}_{be} \\ &- F_{0e} - F_{1e}P_{0te} + (K_{0e} + K_{1e}P_{0te}) \\ &\times x_{te} + (B_{0te} + B_{1te}P_{0te})\dot{x}_{te}]\,r_e \qquad (3.7c)\\ \tau_{1e} =& n_e[F_{1e} + K_{1e}x_{be} - B_{1be}\dot{x}_{be} \\ &+ F_{1e} - K_{1e}x_{te} + B_{1te}\dot{x}_{te}]r_e. \qquad (3.7d)\end{aligned}$$

In (3.7), B_{0ts}, B_{1ts}, B_{0bs}, B_{1bs}, B_{0be}, B_{1be}, B_{0te}, and B_{1te} are the appropriate coefficients from (2.3), depending on whether the PMs are being inflated or deflated.

The dynamics of a planar arm are summarized in the Appendix. Combining (3.6) and (3.7) with (A1)–(A5), we can arrive at the following model for the planar arm actuated by four PMs as in Fig. 3:

$$\begin{bmatrix}\ddot{\theta}_1\\ \ddot{\theta}_2\end{bmatrix} = \begin{bmatrix}a_1\\ a_2\end{bmatrix} + G\begin{bmatrix}\Delta p_s\\ \Delta p_e\end{bmatrix} \qquad (3.8)$$

where

$$\begin{bmatrix}a_1\\ a_2\end{bmatrix} = D^{-1}\left(-C\dot{\theta} - f + \begin{bmatrix}\tau_{0s}\\ \tau_{0e}\end{bmatrix}\right) \qquad (3.9)$$

and

$$G = D^{-1}\begin{bmatrix}\tau_{1s} & 0\\ 0 & \tau_{1e}\end{bmatrix}. \qquad (3.10)$$

Note that a_1, a_2, and G are functions of θ_1, $\dot{\theta}_1$, θ_2, and $\dot{\theta}_2$.

The planar arm actuated by $n_s + n_e$ pairs of PMs in opposing pair configuration modeled as in (3.8) is now in a form which can be handled by multiple-input sliding-mode control methods.

IV. PM Nominal Pressures for Desired Equilibrium Position of Planar Arm

In this section, we find nominal pressures P_{0ts}, P_{0bs}, P_{0te}, P_{0be} such that the arm has an equilibrium point at a desired constant shoulder angle θ_{1eq} and an elbow angle θ_{2eq}. We do this in order that, if control is lost, the arm will revert to the desired equilibrium position. Another reason to do this is to produce desired stiffness in the joint. In order to find proper nominal pressures, we find relationships between them to balance the steady-state clockwise and counterclockwise torques about the shoulder and elbow as functions of the desired equilibrium joint angles. For this analysis, we assume all PM coefficients are exactly known. If they are not, see the end of this section.

From (3.1)–(3.3) and (3.7), the total steady-state clockwise and counterclockwise torques about the shoulder in Fig. 3 are

$$\begin{aligned}\tau_{scw} =& n_s\left[F_{0s}+F_{1s}P_{0bs}-(K_{0s}+K_{1s}P_{0bs})\right.\\ &\left.\times r_s\left(\frac{\pi}{2}-\theta_{1eq}\right)\right]r_s+\tau_{12} \qquad (4.1a)\\ \tau_{sccw} =& n_s\left[F_{0s}+F_{1s}P_{0ts}-(K_{0s}+K_{1s}P_{0ts})\right.\\ &\left.\times r_s\left(\theta_{1eq}+\frac{\pi}{2}\right)\right]r_s \qquad (4.1b)\end{aligned}$$

where

$$\tau_{12}=(m_1l_{c1}+m_2l_1)g\cos\theta_{1eq}+m_2l_{c2}g\cos(\theta_{1eq}+\theta_{2eq}) \qquad (4.2)$$

is the clockwise torque imparted to the shoulder by gravity and r_s is the radius of the shoulder pulley.

Equating the clockwise and counterclockwise torques results in the following relationship between P_{0bs} and P_{0ts}:

$$P_{0ts}=m_sP_{0bs}+c_s \qquad (4.3)$$

where

$$m_s=\frac{\left[F_{1s}-K_{1s}r_s\left(\frac{\pi}{2}-\theta_{1eq}\right)\right]}{\Delta_s} \qquad (4.4a)$$

$$c_s=\frac{\left(2K_{0s}r_s\theta_{1eq}+\frac{\tau_{12}}{n_sr_s}\right)}{\Delta_s} \qquad (4.4b)$$

and

$$\Delta_s=F_{1s}-K_{1s}r_s\left(\theta_{1eq}+\frac{\pi}{2}\right) \qquad (4.5)$$

Similarly, the total steady-state clockwise and counterclockwise torques about the elbow are

$$\begin{aligned}\tau_{ecw} =& n_e\left[F_{1e}P_{0te}-(K_{0e}+K_{1e}P_{0te})\right.\\ &\left.\times r_e(\pi-\theta_{2eq})\right]r_e+\tau_2 \qquad (4.6a)\\ \tau_{eccw} =& n_e\left[F_{1e}P_{0be}-(K_{0e}+K_{1e}P_{0be})r_e\theta_{2eq}\right]r_e \qquad (4.6b)\end{aligned}$$

where

$$\tau_2=m_2l_{c2}g\cos(\theta_{1eq}+\theta_{2eq}) \qquad (4.7)$$

is the clockwise torque imparted to the elbow by gravity, and r_e is the radius of the elbow pulley.

Equating these torques results in the following relationship between P_{0be} and P_{0te}:

$$P_{0be}=m_eP_{0te}+c_e \qquad (4.8)$$

where

$$m_e=\frac{[F_{1e}-K_{1e}r_e(\pi-\theta_{2eq})]}{\Delta_e} \qquad (4.9a)$$

$$c_e=\frac{\left[K_{0e}r_e(2\theta_{2eq}-\pi)+\frac{\tau_2}{n_er_e}\right]}{\Delta_e} \qquad (4.9b)$$

and

$$\Delta_e=F_{1e}-K_{1e}r_e\theta_{2eq}. \qquad (4.10)$$

Thus, we have relationships between the nominal bicep and tricep pressures for shoulder and elbow joints that depend on the system coefficients and the desired equilibrium angles. Therefore, for a given shoulder equilibrium angle θ_{1eq}, one of the nominal shoulder pressures (say P_{0bs}) could be chosen arbitrarily in (4.3), and the other (P_{0ts}) determined by this choice. Similarly, for a given elbow equilibrium angle θ_{2eq}, P_{0te} could be chosen arbitrarily in (4.8), and P_{0be} determined by this choice. These nominal pressures will be used in (3.4) and (3.5) to determine the total PM pressures. The significance of these nominal pressures is that if the control inputs $\Delta p_s=\Delta p_e=0$, the arm orientation reverts to the equilibrium angles θ_{1eq}, θ_{2eq}. Thus, the arm is well-behaved even if the control loop is opened.

In practice, if the exact PM coefficients are unknown, these pressures could be easily determined experimentally, e.g., by first setting, say P_{0bs} and P_{0te} to some nominal values, then manually adjusting P_{0ts} and P_{0be} until the desired equilibrium arm orientation is obtained. In our following simulations, we arbitrarily choose $\theta_{1eq}=-\pi/4$ and $\theta_{2eq}=\pi/2$.

It should be noted that larger nominal pressures increase joint stiffness and decrease joint compliance. An advantage of decreasing joint compliance is reduced susceptibility of the arm to impact disturbances such as unintended hitting of the arm or, in case of exoskeletons, unintended limb motions, which might decrease tracking accuracy. A disadvantage of decreased compliance is less flexibility in the arm, increasing the chances of discomfort and possible damage when the arm comes in contact with humans or equipment, or in the case of exoskeletons, greater discomfort in the event of limb spasms.

Nominal pressures are also important when considering the total PM pressures that will be necessary to accomplish a given task. PM pressures are practically limited to lie between maximum and minimum values, depending on the PM. However, a given task of the arm can be accomplished with any nominal pressure, if joint stiffness is not a concern. To keep all PM pressures within the allowable range, it is generally necessary to adjust the nominal PM input pressures as well as the number of parallel PMs actuating a joint. The necessary pressures will depend on the tracking task and the mass to be actuated by the arm. For instance, in the simulations at the end of this paper, the link masses are both 10 kg. In order to accompish

the tracking tasks while keeping all PM pressures within the allowable range for the PMs under consideration, i.e., $206.844 \leq P \leq 620.532$ kPa $(30 \leq P \leq 90$ psi$)$, it is necessary to use six pairs of PMs actuating the shoulder and three pairs for the elbow, with $P_{0bs} = P_{0te} = 310.3$ kPa $(45$ psi$)$, $P_{0ts} = 449.6$ kPa $(65.2$ psi$)$, and $P_{0be} = 310.5$ kPa $(45$ psi$)$, satisfying (4.3) and (4.8).

V. Two-Input Sliding-Mode Control for Planar Arm Actuated by Four PMs

Consider the model (3.8)–(3.10) of the planar arm actuated by four PMs. Because of our imperfect knowledge of coefficients F, K, and B for all PMs, we must assume that $a_1(\theta, \dot{\theta})$, $a_2(\theta, \dot{\theta})$, and $G(\theta, \dot{\theta})$ are imprecise. Let the extent of the imprecisions on a_1, a_2, and G be bounded by known continuous functions of θ_1, $\dot{\theta}_1$, θ_2, and $\dot{\theta}_2$. The control problem is to determine torques τ_s and τ_e to force the end effector (i.e., the end of the forearm) to follow a desired path in the spatial variables x and y (see Fig. A1 in the Appendix) in the presence of model imprecision on a_1, a_2, and G. It is straightforward to convert this into a tracking problem for the shoulder and elbow joint angles $\theta_1(t)$ and $\theta_2(t)$ using the inverse kinematics of the arm (A6).

Assume we have estimates $\widehat{a}_1, \widehat{a}_2$ of a_1 and a_2 such that

$$|\widehat{a}_i - a_i| \leq A_i \tag{5.1}$$

for some known positive functions A_i, $i = 1, 2$. Further assume the control gain matrix G is unknown but that we have an estimate $\widehat{G}$ for it such that

$$G = (I + \Delta)\widehat{G} \tag{5.2}$$

with $|\Delta_{ij}| \leq \delta_{ij}$ for $i, j = 1, 2$ where δ_{ij} are known positive functions. Also, we assume that G is nonsingular over the entire state space, and that $\widehat{G}$ is invertible, continuously dependent on the parametric uncertainty, and such that $\widehat{G} = G$ in the absence of parametric uncertainty.

Let $\theta_1^*(t)$ and $\theta_2^*(t)$ be smooth functions of time that represent the desired trajectories for the shoulder and elbow angles. Consider the two sliding surfaces $\sigma_i = 0$, $i = 1, 2$ with

$$\sigma_i = \dot{\widetilde{\theta}}_i + \mu_i \widetilde{\theta}_i = \dot{\theta}_i - \dot{\theta}_{ri} \tag{5.3}$$

where $\widetilde{\theta}_i = \theta_i - \theta_i^*$ are the two tracking errors, μ_1 and μ_2 are positive scalar design parameters, and

$$\dot{\theta}_{ri} = \dot{\theta}_i^* - \mu_i \widetilde{\theta}_i. \tag{5.4}$$

Then, the tracking problem can be translated into finding inputs $[\Delta p_s \ \Delta p_e]^T$ that verify the individual sliding conditions

$$\frac{1}{2}\frac{d}{dt}\sigma_i^2 \leq -\eta_i |\sigma_i| \tag{5.5}$$

with $\eta_i > 0$ in the presence of parametric uncertainty.

Let the sliding-mode control law be given by

$$\begin{bmatrix} \Delta p_s \\ \Delta p_e \end{bmatrix} = \widehat{G}^{-1} \left(\begin{bmatrix} \dot{\theta}_{r1} \\ \dot{\theta}_{r2} \end{bmatrix} - \begin{bmatrix} \widehat{a}_1 \\ \widehat{a}_2 \end{bmatrix} - \begin{bmatrix} k_1 \mathrm{sgn}(\sigma_1) \\ k_2 \mathrm{sgn}(\sigma_2) \end{bmatrix} \right) \tag{5.6}$$

where k_1 and k_2 are positive constants. Then, since

$$\begin{aligned} \dot{\sigma}_1 =& \widehat{a}_1 - a_1 + \Delta_{11}(\dot{\theta}_{r1} - \widehat{a}_1) + \Delta_{12}(\dot{\theta}_{r1} - \widehat{a}_2) \\ & - \Delta_{12} k_2 \mathrm{sgn}(\sigma_2) - (1 + \Delta_{11}) k_1 \mathrm{sgn}(\sigma_1) \end{aligned} \tag{5.7a}$$

$$\begin{aligned} \dot{\sigma}_2 =& \widehat{a}_2 - a_2 + \Delta_{21}(\dot{\theta}_{r2} - \widehat{a}_1) + \Delta_{22}(\dot{\theta}_{r2} - \widehat{a}_2) \\ & - \Delta_{21} k_1 \mathrm{sgn}(\sigma_1) - (1 + \Delta_{22}) k_2 \mathrm{sgn}(\sigma_2) \end{aligned} \tag{5.7b}$$

the sliding conditions (5.5) are verified if

$$\begin{aligned} (1 - \delta_{11}) k_1 \geq & A_1 + \delta_{11}|\dot{\theta}_{r1} - \widehat{a}_1| \\ & + \delta_{12}|\dot{\theta}_{r1} - \widehat{a}_2| - \delta_{12} k_2 \end{aligned} \tag{5.8a}$$

$$\begin{aligned} (1 - \delta_{22}) k_2 \geq & A_2 + \delta_{21}|\dot{\theta}_{r2} - \widehat{a}_1| \\ & + \delta_{22}|\dot{\theta}_{r2} - \widehat{a}_2| - \delta_{21} k_1 \end{aligned} \tag{5.8b}$$

and, in particular, if k_1 and k_2 are chosen such that

$$\begin{aligned} (1 - \delta_{11}) k_1 + \delta_{12} k_2 = & A_1 + \delta_{11}|\dot{\theta}_{r1} - \widehat{a}_1| \\ & + \delta_{12}|\dot{\theta}_{r1} - \widehat{a}_2| + \eta_1 \end{aligned} \tag{5.9a}$$

$$\begin{aligned} (1 - \delta_{22}) k_2 + \delta_{21} k_1 = & A_2 + \delta_{21}|\dot{\theta}_{r2} - \widehat{a}_1| \\ & + \delta_{22}|\dot{\theta}_{r2} - \widehat{a}_2| + \eta_2 \end{aligned} \tag{5.9b}$$

The Frobenius–Perron theorem [28] guarantees that (5.9a) and (5.9b) have a unique nonnegative solution $[k_1, k_2]$. Therefore, the control law (5.6) with k_1, k_2 defined by (5.9a) and (5.9b) satisfies the sliding conditions (5.5) in the presence of parametric uncertainties bounded as in (5.1) and (5.2).

The control law (5.6) is known to cause chattering due to the discontinuities across the sliding surfaces. To reduce this, we introduce boundary layers in the vicinity of the sliding surfaces. Inside the boundary layers, the control laws are linear and continuous. Outside the boundary layers, the control laws have the form given in (5.6). The complete multiple-input sliding-mode control law for the arm is given by

$$\begin{bmatrix} \Delta p_s \\ \Delta p_e \end{bmatrix} = \widehat{G}^{-1} \left(\begin{bmatrix} \dot{\theta}_{r1} \\ \dot{\theta}_{r2} \end{bmatrix} - \begin{bmatrix} \widehat{a}_1 \\ \widehat{a}_2 \end{bmatrix} - \begin{bmatrix} k_1 \mathrm{sat}\left(\frac{\sigma_1}{\Gamma_1}\right) \\ k_2 \mathrm{sat}\left(\frac{\sigma_2}{\Gamma_2}\right) \end{bmatrix} \right) \tag{5.10}$$

where

$$\mathrm{sat}(y) = \begin{cases} y, & |y| \leq 1 \\ \mathrm{sgn}(y), & \text{otherwise} \end{cases} \tag{5.11}$$

and Γ_1 and Γ_2 are the boundary layer thicknesses, i.e., the boundary layers are defined by

$$L_1 = \left\{ (\theta_1, \dot{\theta}_1) : \left| \sigma_1(\theta_1, \dot{\theta}_1) \right| \leq \Gamma_1 \right\} \tag{5.12a}$$

$$L_2 = \left\{ (\theta_2, \dot{\theta}_2) : \left| \sigma_2(\theta_2, \dot{\theta}_2) \right| \leq \Gamma_2 \right\}. \tag{5.12b}$$

Thus, when the state trajectories are outside their respective boundary layers, the trajectories approach and reach the boundary layers in finite times due to (5.7a) and (5.7b) when k_1, k_2 are chosen to satisfy (5.9a) and (5.9b). Once inside the boundary layers, the state trajectories θ_1 and θ_2 are governed by (5.3), i.e., taking the Laplace transform of $\widetilde{\theta}_i(t)$ we have

$$\widetilde{\theta}_i(s) = \frac{1}{s + \mu_i} \sigma_i(s) \tag{5.13}$$

TABLE I
PM COEFFICIENT SETS USED FOR THE SIMULATIONS. $Si(Ei)$ = shoulder (elbow) PM COEFFICIENTS FOR ACTUAL PM COEFFICIENT SET i

Coefficient	**Ideal**	$S1$	$E1$	$S2$	$E2$	$S3$	$E3$
$F_0(\times 10^2)$	1.79	1.53	2.58	0.984	2.3	1.69	2.40
F_1	1.39	0.763	1.67	1.49	0.812	1.99	0.722
K_0	5.71	7.17	7.70	6.86	8.25	5.52	6.75
$K_1(\times 10^{-2})$	3.07	4.28	2.18	4.49	4.35	2.82	2.70
B_{0i}	1.01	0.794	0.965	1.26	1.11	1.36	1.35
$B_{1i}(\times 10^{-3})$	6.91	5.19	4.02	8.57	5.21	7.08	6.93
$B_{0d}(\times 10^{-1})$	6.00	8.60	8.11	5.59	8.24	4.22	7.26
$B_{1d}(\times 10^{-4})$	− 8.03	− 5.07	− 8.53	− 9.11	− 8.14	− 9.41	− 7.46

which, together with the fact that $|\sigma_i| \leq \Gamma_i \; \forall t \geq t_1$ with t_1 finite, yields

$$\lim_{t_0 \to \infty} \sup_{t \geq t_0} |\theta_i(t) - \theta_i^*(t)| \leq \frac{\Gamma_i}{\mu_i} \tag{5.14}$$

for $i = 1, 2$.

Therefore, we have that the sliding-mode control law (5.10) guarantees that the state trajectories reach their respective boundary layers in finite times whatever the initial states, and inside the boundary layers constrains trajectories to stay inside them for all later time and approach neighborhoods of $\tilde{\theta}_i = 0$ asymptotically as $t \to \infty$. Asymptotic tracking of the shoulder and elbow angles to within guaranteed accuracy is therefore obtained in spite of modeling errors which may be present in PM coefficients, masses, distances, etc. Thus, the desired spatial path is followed by the end effector within an error bound.

VI. SIMULATION RESULTS

The planar arm of Figs. 3 and A1 with opposing-pair PMs of the type described in Section II actuating the shoulder and elbow joints is simulated using a fourth-order Runge–Kutta algorithm with a step size of 0.01 s. Let $l_1 = l_2 = 0.46$ m, $l_{c1} = l_{c2} = 0.23$ m, $m_1 = m_2 = 10$ kg, $r_s = 7.62$ cm, $r_e = 5.08$ cm, $n_s = 6$, and $n_e = 3$. For these simulations, we assume all physical quantities of the arm, i.e., masses, lengths, etc., are exactly known, but that the PM coefficients, i.e., F, K, and B are not known with precision. Assume all 12 shoulder PMs (six pairs) are matched to each other, but not to the elbow PMs. Similarly assume all six elbow PMs (three pairs) are matched to each other, but not to the shoulder PMs.

The sliding-mode controller is designed according to (5.10) with $\hat{a}_1$ and $\hat{a}_2$ given by (3.9) and $\hat{G}$ given by (3.10) using ideal values for all F, K, and B coefficients (see Section II). To investigate robustness of the sliding-mode controller, we randomly choose three sets of actual (nonideal) F, K, and B coefficients from a uniform distribution within ±50% of their nominal values. The coefficients used are listed in Table I.

The coefficients listed in Table I are those that produced the greatest tracking error (while maintaining a random selection), so that we could see how close to the predicted error bounds (5.14) the actual tracking errors were. Other choices for coefficients produced less tracking error, so are not reported. In the process of choosing which sets of coefficients to use for the simulations, it was noticed that tracking error was by far the most sensitive to variations in the coefficient, F_1. This is perhaps not surprising, since from (2.1), (2.4) the PM contractile force F is directly proportional to this coefficient, and F has a more direct effect on the PM force than the other coefficients (K_0, K_1, B_0, and B_1).

For all simulations, we use $\mu_i = 5.0$ and $\Gamma_i = 1.0$. From simulations with parametric uncertainties within the ±50% range, we find that $A_1 = 12.5$ and $A_2 = 15.0$ satisfy inequalities (5.1). From (5.2), we also have $\Delta = [\Delta_{ij}]$ where

$$|\Delta_{ij}| \leq \delta_{ij} = \begin{cases} 0.5, & i = j \\ 0, & i \neq j. \end{cases} \tag{6.1}$$

Using these values and the simulated functions $|\dot{\theta}_{ri} - \hat{a}_i|$, $i = 1, 2$, we find $k_i = 50$, $i = 1, 2$, satisfies (5.8), resulting in closed-loop stability and convergence of the trajectories to the interior of the boundary layers and a guaranteed tracking precision of $\Gamma_i/\mu_i = 0.2$ radians for both joints. In addition, let $\theta_{1eq} = -\pi/4$, $\theta_{2eq} = \pi/2$, $P_{0bs} = P_{0te} = 310.3$ kPa (45 psi), resulting in $P_{0ts} = 449.6$ kPa (65.2 psi) and $P_{0be} = 310.5$ kPa (45 psi), satisfying (4.3) and (4.8). With these nominal pressures and with n_s, n_e as earlier, all PM pressures remain in the allowable range $206.844 \leq P \leq 620.532$ kPa ($30 \leq P \leq 90$ psi) for all control tasks in this section.

We investigate controller performance for three tracking tasks for the end effector in x–y space: a sinusoidal spline, a vertical line, and a circle.

A. Sinusoidal Spline

The desired spatial path is given by

$$x_d(t) = 0.1524 + 0.1219t \text{ m} \tag{6.2a}$$

$$y_d(t) = 0.396\,24 + 0.243\,84 \sin\left(0.4\pi t - \frac{\pi}{2}\right) \text{ m} \tag{6.2b}$$

where $0 \leq t \leq 5$ s.

The spatial tracking performance for the true plant with PM coefficients in set 1 is shown in Fig. 4. Tracking performance when PMs are described by coefficient sets 2 and 3 are similar to Fig. 4. It will be noted that there is some spatial tracking error, which is to be expected due to the parameter errors. An initial transient can also be seen, due to the initial pressure adjustment that is necessary to produce accurate tracking.

Fig. 5 shows the control efforts Δp_s and Δp_e that produced the tracking performance in Fig. 4. It will be noted that with the nominal pressures P_{0ts}, P_{0bs}, P_{0te}, and P_{0be} given earlier, the PM input pressures remain within the allowable range for these PM's. The elbow angle tracking error (which is larger than the shoulder angle tracking error in this case) for coefficient sets 1, 2, and 3 is shown in Fig. 6. It is seen that for all systems the tracking error is within predicted bounds, i.e.,

$$\lim_{t_0 \to \infty} \sup_{t \geq t_0} |\theta_i(t) - \theta_i^*(t)| \leq \frac{\Gamma_i}{\mu_i} = 0.2 \text{ radians.} \tag{6.3}$$

This tracking error is obtained after the initial transients have died away.

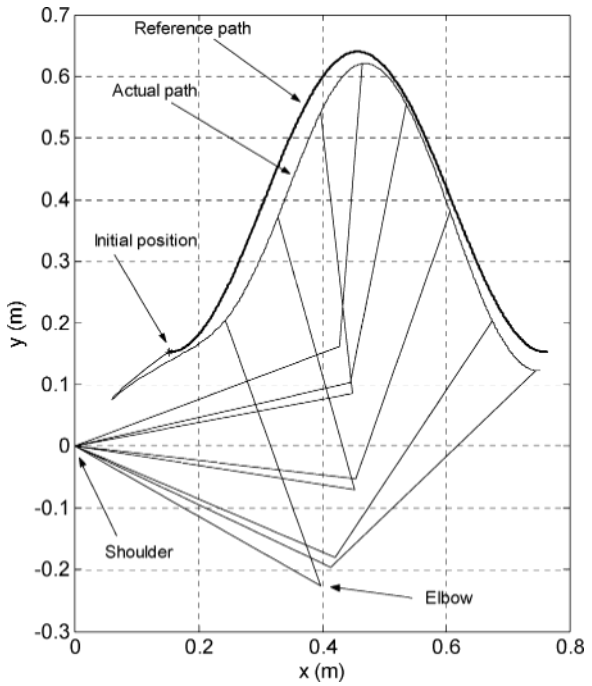

Fig. 4. Spatial tracking behavior, PMs in coefficient set 1, $m_1 = m_2 = 10$ kg.

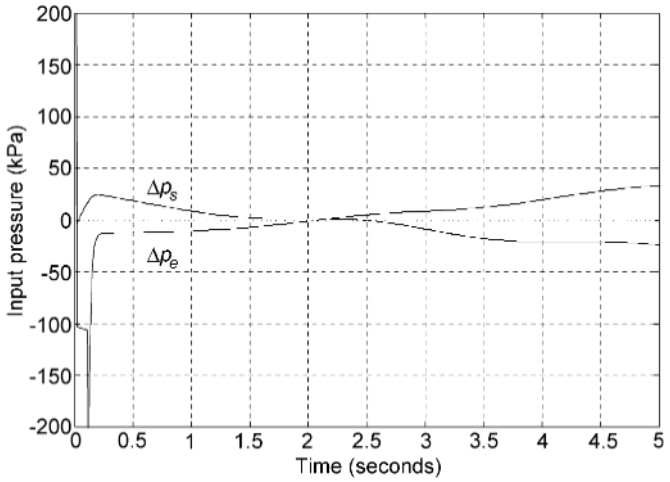

Fig. 5. Control effort producing tracking performance of Fig. 4.

B. Vertical Line

The desired spatial path for the vertical line is given by:

$$x_d(t) = 0.6096 \text{ m} \tag{6.4a}$$

$$y_d(t) = 0.396\,24 + 0.243\,84 \sin\left(0.4\pi t - \frac{\pi}{2}\right) \text{ m}. \tag{6.4b}$$

The spatial tracking performance for PMs with coefficients in set 3 is shown in Fig. 7. Tracking performance for other sets is similar. The corresponding control effort is shown in Fig. 8. The elbow angle tracking error (which is larger than the shoulder angle tracking error in this case) for PMs with coefficients in sets 1, 2, and 3 is shown in Fig. 9. It is seen that for all systems the tracking error is within predicted bounds and PM pressures remain within the allowable range.

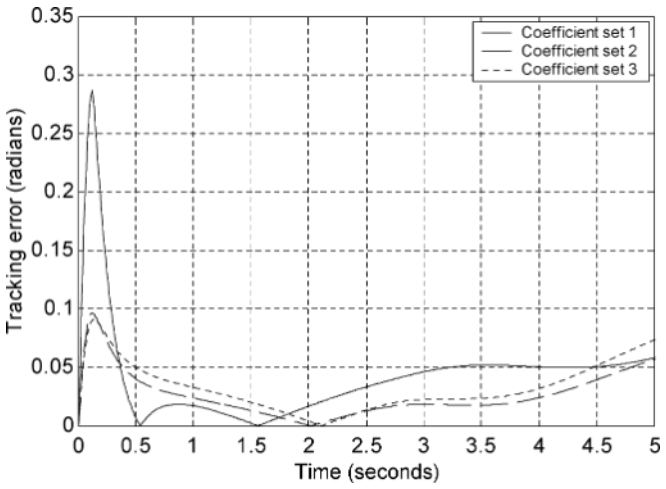

Fig. 6. Elbow angle tracking errors for three different plants (PM coefficient sets 1, 2, and 3), sinusoidal spline reference trajectory $m_1 = m_2 = 10$ kg.

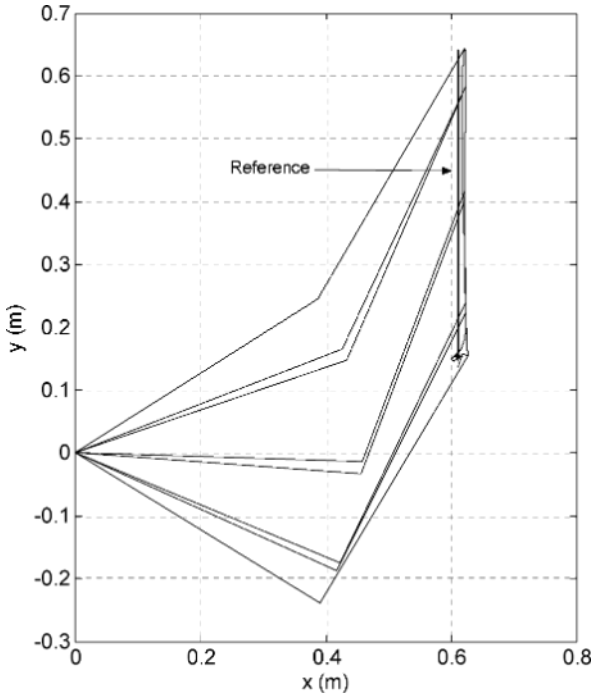

Fig. 7. Spatial tracking behavior, PMs in coefficient set 3, $m_1 = m_2 = 10$ kg.

C. Circle

The desired spatial path for the circle is given by:

$$x_d(t) = 0.365\,76 + 0.3048 \sin(0.4\pi t - 0.7754)) \text{ m} \tag{6.5a}$$

$$y_d(t) = 0.365\,76 + 0.3048 \cos(0.4\pi t + 2.3462) \text{ m}. \tag{6.5b}$$

The spatial tracking performance for PMs with coefficients in set 1 is shown in Fig. 10. The corresponding control effort is shown in Fig. 11. The elbow angle tracking error (which is larger than the shoulder angle tracking error in this case) for PMs with coefficients in sets 1, 2, and 3 is shown in Fig. 12. It is seen that for all systems the tracking error is within predicted bounds and PM pressures remain within the allowable range.

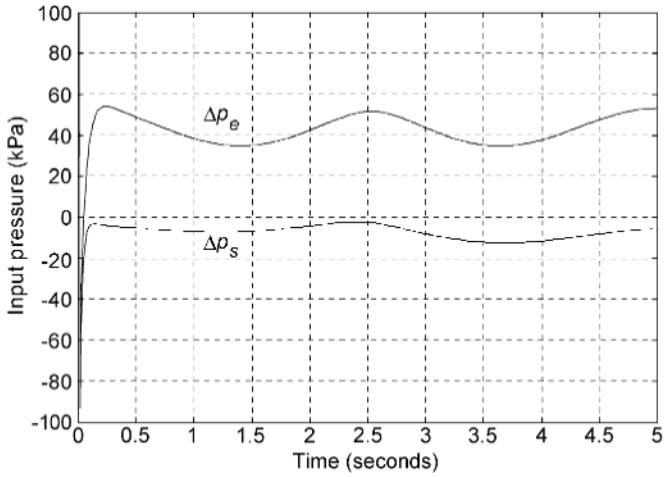

Fig. 8. Control effort producing tracking performance of Fig. 7.

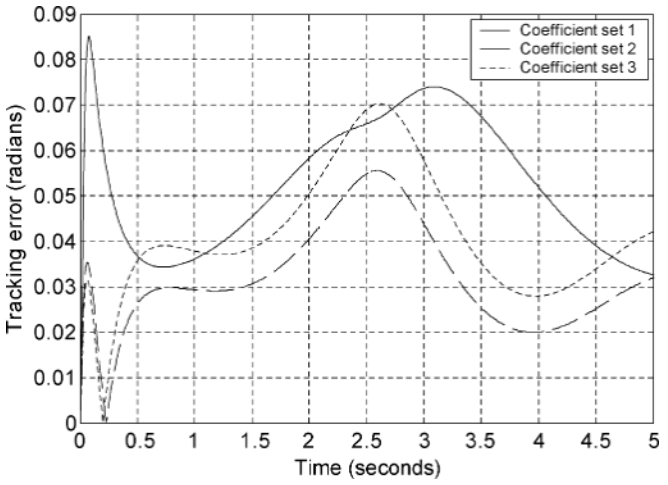

Fig. 9. Elbow angle tracking errors for three different plants (PM coefficient sets 1, 2, and 3), vertical line reference trajectory, $m_1 = m_2 = 10$ kg.

D. Sinusoidal Spline, Doubled Mass

In practical applications, it may be expected that the mass actuated by the arm will change. To investigate the robustness of the sliding controller to changing masses, we increased the arm masses m_1, m_2 each by a factor of 2 (to 20 kg) and used the same controller as shown previously to track the sinusoidal spline reference trajectory (6.2). Both the shoulder and elbow angle tracking errors are again within predicted bounds, indicating that the sliding-mode controller is robust to changes in mass.

Fig. 13 shows the control effort produced by the sliding controller for this plant. It is seen that with the previous nominal pressures, the PM pressures remain within the allowable range for the duration of the control process.

VII. Discussion and Conclusion

A two-input sliding-mode controller has been designed for a 2-DOF planar arm assembly with highly nonlinear pneumatic muscle actuators in opposing pair configurations actuating the shoulder and elbow joints. Designation of these joints as shoulder and elbow is arbitrary and nominal; however, it is convenient for considering applications in which pneumatic muscle actuated devices could provide joint loading to generate or assist extremity motion, or maintain extension of muscles with contractures.

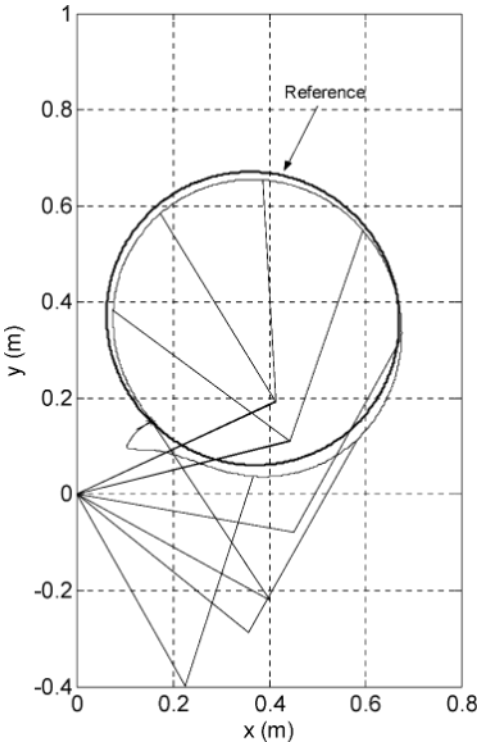

Fig. 10. Spatial tracking behavior, PMs in coefficient set 1, $m_1 = m_2 = 10$ kg.

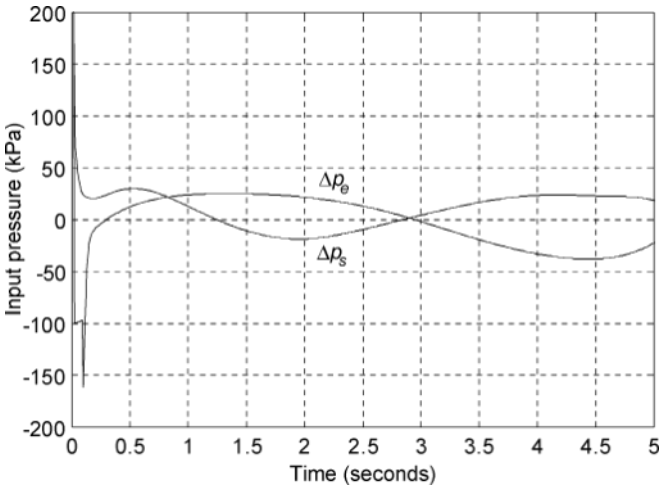

Fig. 11. Control effort producing tracking performance of Fig. 10.

The control input for the planar assembly enters the process through nonlinear spring and friction coefficients and a nonlinear contractile force term that are contained within a mathematical model for the pneumatic muscle actuators. A dynamic model for the arm with four groups of PM actuators is derived, and this is put in a form suitable for sliding-mode control. A relationship between nominal PM pressures is derived to give stable arm behavior in the absence of any control signal, and desired joint stiffness.

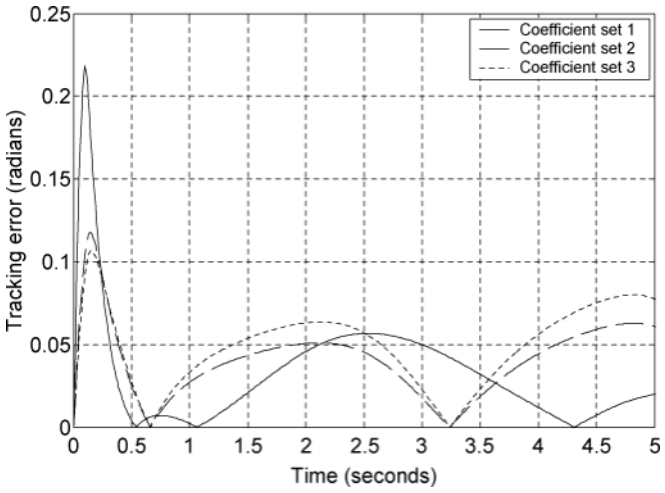

Fig. 12. Elbow angle tracking errors for three different plants (PM coefficient sets 1, 2, and 3), circle reference trajectory, $m_1 = m_2 = 10$ kg.

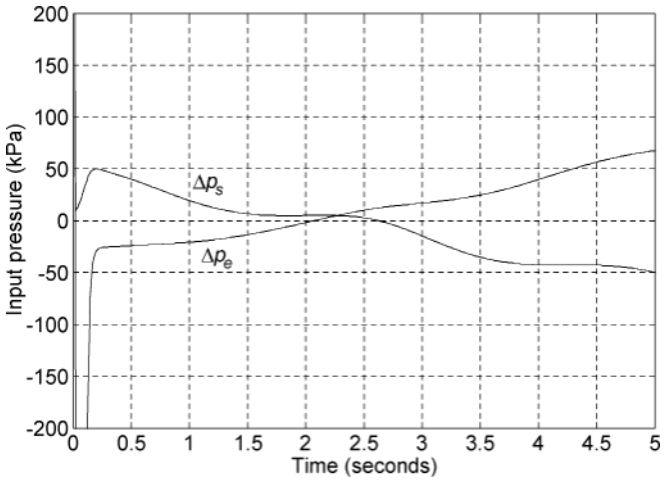

Fig. 13. Control effort, sinusoidal spline reference trajectory, coefficients in set 1, $m_1 = m_2 = 20$ kg.

Simulations of closed-loop tracking were performed with sinusoidal spline, vertical line, and circle paths desired for the end effector. These paths are generic in nature; however, they can serve well as potential building blocks for an ample variety of more task-oriented end effector paths. Data from the motion biomechanics literature [29], [30], as well as dedicated biomechanical experimentation, could be used to identify actual end effector paths for practical activities such as feeding and grooming.

Closed-loop tracking performance, resulting from simulations, is in line with theoretically predicted behavior. Closed-loop tracking with several sets of PM coefficients within a $\pm 50\%$ range of ideal are shown to agree with theoretical results. The controller is also shown to be robust for a 100% change in arm masses. Thus, sliding-mode control is shown to be a very promising method for control of systems containing pneumatic muscle actuators, including devices that could potentially benefit persons with neuromuscular or musculoskeletal pathologies.

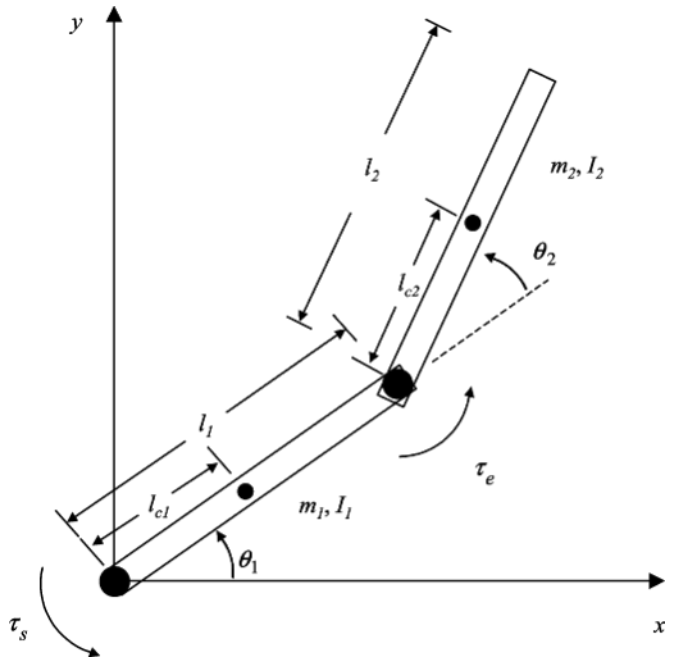

Fig. A1. Planar arm.

APPENDIX

Consider the manipulator configuration shown in Fig. A1, which depicts a two-joint planar arm. In this figure, θ_i denotes the angle of joint i, m_i denotes the mass of link i, l_i denotes the length of link i, l_{ci} denotes the distance from the previous joint to the center of mass of link i (center of mass is denoted by a small dot), and I_i denotes the moment of inertia of link i about an axis coming out of the page, passing through the center of mass of link i.

The dynamics of this system are well-known [31] to be described by the following:

$$D(\theta)\ddot{\theta} + C(\theta, \dot{\theta})\dot{\theta} + f(\theta) = \tau \tag{A1}$$

where $\theta = [\theta_1, \theta_2]^T$ and $\tau = [\tau_s, \tau_e]^T$ is a matrix of input torques. The nonsingular inertia matrix $D(\theta)$ is

$$D(\theta) = \begin{bmatrix} d_{11} & d_{12} \\ d_{21} & d_{22} \end{bmatrix} \tag{A2}$$

where

$$d_{11} = m_1 l_{c1}^2 + m_2 \left(l_1^2 + l_{c2}^2 + 2 l_1 l_{c2} \cos\theta_2\right) + I_1 + I_2 \tag{A3a}$$

$$d_{12} = d_{21} = m_2 \left(l_{c2}^2 + l_1 l_{c2} \cos\theta_2\right) \tag{A3b}$$

$$d_{22} = m_2 l_{c2}^2 + I_2 \tag{A3c}$$

and $I_i = m_i l_{ci}^2$, $i = 1, 2$. The matrix $C(\theta, \dot{\theta})$ is given as

$$C(\theta, \dot{\theta}) = \begin{bmatrix} h\dot{\theta}_2 & h\dot{\theta}_2 + h\dot{\theta}_1 \\ -h\dot{\theta}_1 & 0 \end{bmatrix} \tag{A4}$$

with $h = -m_2 l_1 l_{c2} \sin\theta_2$. The vector $f(\theta)$ is given by $f(\theta) = [f_1, f_2]^T$ where

$$f_1 = (m_1 l_{c1} + m_2 l_1) g \cos\theta_1 + m_2 l_{c2} g \cos(\theta_1 + \theta_2) \tag{A5a}$$

$$f_2 = m_2 l_{c2} g \cos(\theta_1 + \theta_2) \tag{A5b}$$

and g is the acceleration of gravity.

If desired end-effector spatial trajectories $x_d(t)$, $y_d(t)$ are given, then from the inverse kinematics of the planar arm, it is well known [31] that these spatial path requirements are equivalent to required joint trajectories of

$$\theta_2^*(t) = \cos^{-1}\frac{(x_d^2 + y_d^2 - l_1^2 - l_2^2)}{2 l_1 l_2} \tag{A6a}$$

$$\theta_1^*(t) = \tan^{-1}\left(\frac{y_d}{x_d}\right) - \tan^{-1}\left[\frac{(l_2 \sin\theta_2^*)}{(l_1 + l_2\cos\theta_2^*)}\right]. \tag{A6b}$$

REFERENCES

[1] D. G. Caldwell, G. A. Medrano-Cerda, and M. Goodwin, "Control of pneumatic muscle actuators," *IEEE Control Syst. Mag.*, pp. 40–48, Feb. 1995.

[2] C.-P. Chou and B. Hannaford, "Static and dynamic characteristics of McKibben pneumatic artificial muscles," in *Proc. IEEE Robotics Automation Conf.*, 1994, pp. 281–286.

[3] D. W. Repperger, C. A. Phillips, D. C. Johnson, R. D. Harmon, and K. Johnson, "A study of pneumatic muscle technology for possible assistance in mobility," in *Proc. 19th Annu. Int. Conf. IEEE Engineering in Medicine and Biology Soc.*, Chicago, IL, Nov. 1997, pp. 1884–1887.

[4] B. J. Ruthenberg, N. A. Wasylewski, and J. E. Beard, "An experimental device for investigating the force and power requirements of a powered gait orthosis," *J. Rehab. Res. Develop.*, vol. 34, no. 2, pp. 203–213, 1997.

[5] G. R. Johnson and M. A. Buckley, "Development of a new motorized upper limb orthotic system (MULOS)," in *Proc. Rehabilitation Engineering Soc. North America*, Pittsburgh, PA, June 1997, pp. 399–401.

[6] T. R. Lunsford, "Advanced contracture reduction orthosis (CRO)," in *Proc. 19th Annu. Symp. American Academy of Orthotists and Prosthetists*, Las Vegas, NV, 1993, pp. 893–900.

[7] G. Colombo, M. Joerg, R. Schreier, and V. Dietz, "Treadmill training of paraplegic patients using a robotic orthosis," *J. Rehab. Res. Develop.*, vol. 37, no. 6, pp. 693–700, 2000.

[8] B. Tondu and P. Lopez, "Modeling and control of McKibben pneumatic artificial muscle robot actuators," *IEEE Control Syst. Mag.*, vol. 20, pp. 15–38, Apr. 2000.

[9] C. P. Chou and B. Hannaford, "Measurement and modeling of McKibben pneumatic artificial muscles," *IEEE Trans. Robot. Automat.*, vol. 12, pp. 90–102, Feb. 1996.

[10] D. B. Reynolds, D. W. Repperger, C. A. Phillips, and G. Bandry, "Dynamic characteristics of pneumatic muscle," *Ann. Biomed. Eng.*, pp. 310–317, Mar. 2003.

[11] J. Lilly, "Adaptive tracking for pneumatic muscle actuators in bicep and tricep configurations," *IEEE Trans. Neural Syst. Rehab. Eng.*, to be published.

[12] G. A. Medrano-Cerda, C. J. Bowler, and D. G. Caldwell, "Adaptive position control of antagonistic pneumatic muscle actuators," in *Proc. IEEE Int. Conf. Intelligent Robots Systems*, vol. 1, Aug. 1995, pp. 378–383.

[13] R. Q. van der Linde, "Design, analysis, and control of a low power joint for walking robot by phasic activation of McKibben muscle," *IEEE Trans. Robot. Automat.*, vol. 15, pp. 599–604, Aug. 1999.

[14] D. G. Caldwell, G. A. Medrano-Cerda, and M. Goodwin, "Braided pneumatic muscle actuator control of a multi-jointed manipulator," in *Proc. IEEE Systems, Man, and Cybernetics Conf.*, vol. 1, Le Touquet, France, 1993.

[15] T. Hesselroth, K. Sarkar, P. Van der Smagt, and K. Schulten, "Neural network control of a pneumatic robot arm," *IEEE Trans. Syst., Man, Cybern.*, vol. 24, pp. 28–38, Jan. 1994.

[16] D. W. Repperger, C. A. Phillips, and M. Krier, "Controller design involving gain scheduling for a large scale pneumatic muscle actuator," in *Proc. IEEE Conf. Control Applications*, Kohala Coast, HI, Aug. 1999.

[17] S. W. Chan, J. Lilly, D. W. Repperger, and J. E. Berlin, "Fuzzy PD+I learning control for a pneumatic muscle," in *Proc. 2003 IEEE Int. Conf. Fuzzy Systems*, St. Louis, MO, May 2003, pp. 278–283.

[18] X. Chang and J. H. Lilly, "Tracking control of a pneumatic muscle by an evolutionary fuzzy controller," *Intell. Automat. Soft Comput.*, vol. 9, no. 3, pp. 227–244, Sept. 2003.

[19] P. Carbonell, Z. P. Jiang, and D. W. Repperger, "A fuzzy backstepping controller for a pneumatic muscle actuator system," in *Proc. IEEE Int. Symp. Intelligent Control*, Mexico City, Mexico, Sept. 2001, pp. 353–358.

[20] M. Hamerlain, "An anthropomorphic robot arm driven by artificial muscles using a variable structure control," in *Proc. IEEE Int. Conf. Intelligent Robots Systems*, vol. 1, Aug. 1995, pp. 550–555.

[21] D. Cai and H. Yamaura, "A robust controller for manipulator driven by artificial muscle actuator," in *Proc. IEEE Conf. Control Applications*, 1996, pp. 540–545.

[22] D. W. Repperger, K. R. Johnson, and C. A. Phillips, "A VSC position tracking system involving a large sale pneumatic muscle actuator," in *Proc. IEEE Conf. Decision Control*, vol. 4, 1998, pp. 4302–4307.

[23] K. Osuka, T. Kimura, and T. Ono, "H_∞ control of a certain nonlinear actuator," in *Proc. IEEE Conf. Decision Control*, 1990, pp. 370–371.

[24] V. I. Utkin, *Sliding Modes and Their Application in Variable Structure Systems*. Moscow, Russia: MIR, 1978.

[25] J.-J. Slotine and J. A. Coetsee, "Adaptive sliding controller synthesis for nonlinear systems," *Int. J. Control*, vol. 43, no. 6, pp. 1631–1651, 1986.

[26] J.-J. Slotine and S. Sastry, "Tracking control of nonlinear system using sliding surface with application to robot manipulators," *Int. J. Control*, vol. 38, pp. 465–492, 1983.

[27] J.-J. Slotine and W. Li, *Applied Nonlinear Control*. Englewood Cliffs, NJ: Prentice-Hall, 1991.

[28] D. G. Luenberger, *Introduction to Dynamic Systems*. New York: Wiley, 1979.

[29] T. L. Palmieri, K. Petuskey, A. Bagley, S. Takashiba, D. G. Greenhalgh, and G. T. Rab, "Alterations in functional movement after axillary burn scar contracture: A motion analysis study," *J. Burn Care Rehab.*, vol. 24, no. 2, pp. 104–108, 2003.

[30] N. Yang, M. Zhang, C. Huang, and D. Jin, "Synergic analysis of upper limb target-reaching movements," *J. Biomechan.*, vol. 35, no. 6, pp. 739–746, 2002.

[31] J.-J. E. Slotine, "The robust control of robot manipulators," *Int. J. Rob. Res.*, vol. 4, no. 2, pp. 49–64, 1985.

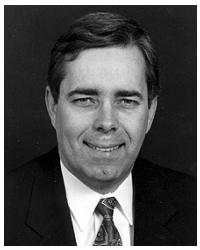

John H. Lilly (S'81–M'82–SM'89) received the Ph.D. degree in computer and systems engineering from Rensselaer Polytechnic Institute, Troy, NY, in 1982.

He is currently the Director of the Controls Laboratory, Electrical and Computer Engineering Department, University of Louisville, Louisville, KY. He recently completed a sabbatical in the Human Sensory Feedback Laboratory, Wright-Patterson Air Force Base, Dayton, OH, where he investigated control methods for pneumatic muscles. He has been a reviewer for several IEEE Transactions and several other related journals. His research interests include adaptive control, fuzzy control, and soft computing applications to control and system identification, including negative-rule fuzzy systems and their identification from data.

Dr. Lilly is a member of Eta Kappa Nu and Sigma Xi, and is a registered professional engineer. He received the UL President's Young Investigator Award for his research.

Peter M. Quesada received the Ph.D. degree in bioengineering from the University of California, Berkeley and San Francisco, in 1991.

He is the Director of the Biokinetics Laboratory, Mechanical Engineering Department, University of Louisville, Louisville, KY, and also the University's Graduate Studies Coordinator for the Mechanical Engineering Department. He has served as a reviewer of biomechanically related manuscripts for several journals. His research interests include the biomechanics of human movement and its applications in rehabilitation, orthopaedics, athletic performance, and ergonomics.

Dr. Quesada has served on the Executive Committee of the Gait and Clinical Movement Analysis Society. He is a member of the American Society of Mechanical Engineers and the American Society of Biomechanics.